

LA-UR-

08-7983

Approved for public release;
distribution is unlimited.

Title: Critical Thickness of High Structural Quality SrTiO₃ Films
Grown on Orthorhombic (101) DyScO₃

Author(s): 11. M. D. Biegalski, D. D. Fong, J. A. Eastman, P. H. Fuoss,
S. K. Streiffer, T. Heeg, J. Schubert, W. Tian, C.T. Nelson, X.
Q. Pan, M. E. Hawley, M. Bernhagen, P. Reiche, R. Uecker,
S. Trolrier-McKinstry, and D. G. Schlom

Intended for: Publication in the Journal of Applied Physics



Los Alamos National Laboratory, an affirmative action/equal opportunity employer, is operated by the Los Alamos National Security, LLC for the National Nuclear Security Administration of the U.S. Department of Energy under contract DE-AC52-06NA25396. By acceptance of this article, the publisher recognizes that the U.S. Government retains a nonexclusive, royalty-free license to publish or reproduce the published form of this contribution, or to allow others to do so, for U.S. Government purposes. Los Alamos National Laboratory requests that the publisher identify this article as work performed under the auspices of the U.S. Department of Energy. Los Alamos National Laboratory strongly supports academic freedom and a researcher's right to publish; as an institution, however, the Laboratory does not endorse the viewpoint of a publication or guarantee its technical correctness.

Critical thickness of high structural quality SrTiO₃ films grown on orthorhombic (101) DyScO₃

M. D. Biegalski,^{1,a)} D. D. Fong,² J. A. Eastman,² P. H. Fuoss,² S. K. Streiffer,³ T. Heeg,⁴ J. Schubert,⁴ W. Tian,⁵ C. T. Nelson,⁵ X. Q. Pan,⁵ M. E. Hawley,⁶ M. Bernhagen,⁷ P. Reiche,⁷ R. Uecker,⁷ S. Trolrier-McKinstry,¹ and D. G. Schlom^{1,b)}

¹Materials Research Institute, Pennsylvania State University, University Park, Pennsylvania 16802-5005, USA

²Materials Science Division, Argonne National Laboratory, Argonne, Illinois 60439, USA

³Center for Nanoscale Materials, Argonne National Laboratory, Argonne, Illinois 60439, USA

⁴Institute of Bio- and Nanosystems (IBNI-IT), and Centre of Nanoelectronic Systems for Information Technology (cni), Forschungszentrum Jülich GmbH, D-52425 Jülich, Germany

⁵Department of Materials Science and Engineering, University of Michigan, Ann Arbor, Michigan 48019-2136, USA

⁶Materials Science and Technology Division (MST-8), Los Alamos National Laboratory, Los Alamos, New Mexico 87545, USA

⁷Institute for Crystal Growth, Max-Born-Straße 2, D-12489 Berlin (Adlershof), Germany

(Received 15 August 2008; accepted 2 November 2008; published online 10 December 2008)

Strained epitaxial SrTiO₃ films were grown on orthorhombic (101) DyScO₃ substrates by reactive molecular-beam epitaxy. The epitaxy of this substrate/film combination is cube on cube with a pseudocubic out-of-plane (001) orientation. The strain state and structural perfection of films with thicknesses ranging from 50 to 1000 Å were examined using x-ray scattering. The critical thickness at which misfit dislocations was introduced was between 350 and 500 Å. These films have the narrowest rocking curves (full width at half maximum) ever reported for any heteroepitaxial oxide film (0.0018°). Only a modest amount of relaxation is seen in films exceeding the critical thicknesses even after postdeposition annealing at 700 °C in 1 atm of oxygen. The dependence of strain relaxation on crystallographic direction is attributed to the anisotropy of the substrate. These SrTiO₃ films show structural quality more typical of semiconductors such as GaAs and silicon than perovskite materials; their structural relaxation behavior also shows similarity to that of compound semiconductor films. © 2008 American Institute of Physics. [DOI: 10.1063/1.3037216]

I. INTRODUCTION

Strain can have a dramatic effect on the properties of thin films. Strain-induced shifts in magnetic,^{1–3} ferroelectric,^{4–11} and superconducting^{12–14} transitions have been reported. For the case of strained SrTiO₃, a ferroelectric transition has been induced in the vicinity of room temperature even though pure, strain-free SrTiO₃ is not ferroelectric at any temperature.⁹ These strained SrTiO₃ films grown on (101) DyScO₃ substrates¹⁵ show a tunability of the dielectric constant at room temperature of 82% at 10 GHz (Ref. 9) and dielectric constant maxima near 20 000 at 500 Hz.¹⁸ Presumably, these properties may change with film thickness, as the strain should relax due to dislocation generation in thicker films. In this paper we investigate both the critical thickness at which (001)_p SrTiO₃ films (where the *p* subscript denotes the pseudocubic Miller index) on (101) DyScO₃ begin to relax and how this relaxation proceeds as the film thickness increases.¹⁹

II. EXPERIMENTAL PROCEDURE

Untwinned single crystals of the orthorhombic perovskite DyScO₃ were grown by the Czochralski method.^{20–24}

These crystals were oriented along the (101) plane and cut into 10 × 10 × 1 mm³ substrates with a surface suitable for epitaxy.²⁵ DyScO₃ is free of phase transitions from room temperature to at least 930 °C and has thermal expansion coefficients comparable to SrTiO₃ and other perovskites.²⁶ This and the low vapor pressure of its constituents make it a suitable substrate for the epitaxial growth of perovskites, including SrTiO₃.

These substrates were cleaned in an ultrasonic bath for 10 min in Micro cleaning solution,²⁷ followed by acetone, isopropyl alcohol, and de-ionized water and then spun dry.²⁸ SrTiO₃ films were grown by reactive molecular-beam epitaxy (MBE) in a Veeco 930 growth chamber to thicknesses of 50, 100, 250, 350, 500, 1000, and 2000 Å. The substrates were heated using a pyrolytic graphite heating element coated with pyrolytic boron nitride²⁹ to a growth temperature of 650 °C (as measured using an optical pyrometer).

The SrTiO₃ films were grown using elemental molecular beams of strontium, titanium, and oxygen. The strontium source was a Veeco low temperature effusion cell loaded with 99.99% pure strontium metal premelted into a titanium crucible.³⁰ The titanium source was a Ti-Ball³¹ sublimation pump.³² To oxidize the films, a molecular beam consisting of a mixture of oxygen and ozone (~10% O₃) was used. The mixture was produced by passing 99.994% pure oxygen through an ASTeX AX8401 ozone generator.³³ Its output was

^{a)}Present address: Center for Nanophase Materials Science, Oak Ridge National Laboratory, Oak Ridge, Tennessee 37830.

^{b)}Electronic mail: bds2@psu.edu.

continuously flowed into the chamber through a Nupro SS-4BMW leak valve³⁴ from a continuously pumped loop of the oxygen-ozone mixture to minimize ozone decomposition. Once past the leak valve, the oxygen-ozone mixture travels down a water-cooled electropolished stainless steel tube (6 mm diameter) that is directed perpendicular to the substrate surface and ends 64 mm from the front of the substrate. During growth, the background pressure of the chamber was increased with this O₂/O₃ mixture from a base pressure of $\sim 5 \times 10^{-9}$ to 3×10^{-6} Torr. This pressure was maintained after growth until the sample had cooled to room temperature to minimize oxygen vacancies.

These films were grown using a shuttered growth technique, similar to that used in the migration-enhanced epitaxy of GaAs.³⁵ For the specific case of SrTiO₃ growth, the heated substrate is exposed to alternating monolayer doses from strontium and titanium molecular beams under a steady flux of oxygen/ozone. The fluxes of the strontium and titanium molecular beams and the stability of these sources were determined using a quartz crystal monitor placed in front of the substrate. The temperature of the strontium and titanium sources are adjusted to give a flux of $\sim 4 \times 10^{13}$ atoms/cm² s from each source, yielding an average growth rate of about 7 Å/min. Reflection high-energy electron diffraction (RHEED) was implemented to optimize the stoichiometry of the growing SrTiO₃ film in real time and monitor the growth.³⁶ A calibration sample was used for RHEED optimization before the growths to ensure the correct stoichiometry at the beginning of the growth.

Structural and microstructural characterizations of the films were then completed. The 2000 Å thick film was riddled with cracks and was not analyzed by x-ray diffraction (XRD). For the remaining films, the lattice parameters and crystalline perfection were examined via x-ray scattering both on beamline 12ID of the Advanced Photon Source and using a Philips X'pert material research diffractometer (MRD).³⁷ The Philips X'pert MRD four-circle x-ray diffractometer was used with a hybrid monochromator (combined graded multilayer mirror and a four-bounce Ge 220 monochromator) on the incident side and a triple axis two-bounce 220 Ge analyzer crystal. For higher intensity only the graded multilayer mirror was used in place of the hybrid monochromator on the incident side. The synchrotron was used to examine the strain state of the thinner films using grazing-incidence x-ray scattering with 24 keV x rays and a fixed incidence angle of 1° (except for the 50 Å film, where higher intensity was needed and an incidence angle of 0.1° was used).³⁸ To determine whether oxidation altered the structure of the as-grown films, the lattice parameters of the 100 Å thick SrTiO₃ film were monitored *in situ* as a function of oxygen partial pressure at 700 °C in a controlled atmosphere environment.³⁹ High-resolution transmission electron microscopy was performed on a JEOL JEM-3011 transmission electron microscope⁴⁰ to image misfit dislocations and determine their Burgers vector. Rutherford backscattering spectrometry (RBS) at the Forschungszentrum Jülich was used to ensure correct stoichiometry and characterize the crystalline quality of the films using RBS channeling. In addition, the film surfaces were imaged using Veeco

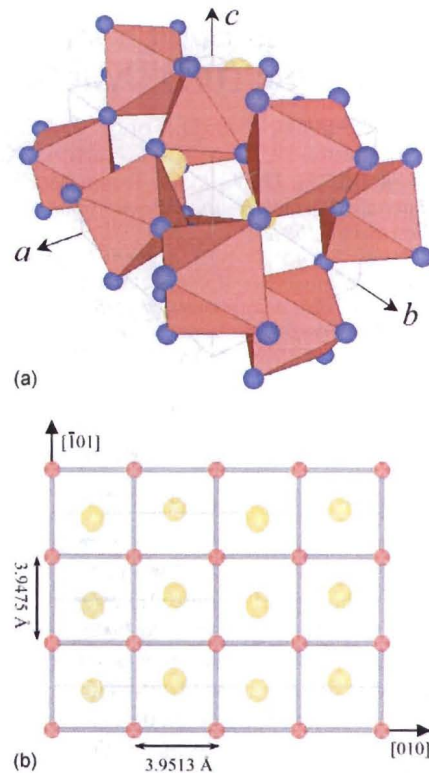


FIG. 1. (Color online) (a) DyScO₃ unit cell in which the ScO₆ coordination polyhedra are shaded, showing the tilts of the octahedra. (b) Schematic of the in-plane rectilinear surface net of the (101) DyScO₃ with a slight asymmetry of the two in-plane directions due to the orthorhombicity of the unit cell. For clarity, the oxygen atoms are not shown.

Metrology multimode IIIA scanning probe microscopes⁴¹ in intermittent contact mode at 0.6 Hz.

III. RESULTS AND DISCUSSION

A. Epitaxial growth of SrTiO₃ films on DyScO₃

The DyScO₃ substrates used in this study have an orthorhombic GdFeO₃ crystal structure with space group *Pnma*. The lattice constants of the substrate were determined from our experiments to be $a=5.7196 \pm 0.0005$ Å, $b=7.9025 \pm 0.0008$ Å, and $c=5.4422 \pm 0.0004$ Å which are in reasonable agreement with previous data.^{17,23,24,26,42–45} The slight difference in lattice constants from literature values is attributed to small stoichiometry differences, as has been noted in other GdFeO₃-type compounds.⁴⁶ This comes about because the composition at which DyScO₃ melts congruently is slightly dysprosium poor compared to the stoichiometric Dy:Sc=1:1 composition.²³ To utilize DyScO₃ as a substrate, the crystal is cut along the (101) plane to match the lattice constant of SrTiO₃. The (101) plane of DyScO₃ consists of a rectilinear surface net spanned by the $[\bar{1}01]$ and $[010]$ DyScO₃ vectors. This surface is schematically shown in Fig. 1, where it can be seen that the DyScO₃ $[\bar{1}01]$ axis, for the measured samples, have a slightly shorter pseudocubic lattice parameter of $\frac{1}{2}[\bar{1}01]=3.9475 \pm 0.0003$ Å, while the pseudocubic lattice spacing along the $[010]$ axis is $\frac{1}{2}[010]=3.9513 \pm 0.0004$ Å. When SrTiO₃ is grown on

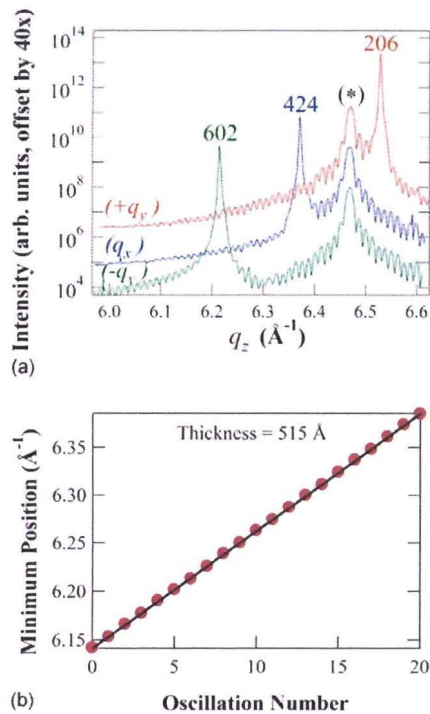


FIG. 2. (Color online) (a) CTRs of a 500 Å thick SrTiO₃ film containing the 204_p-type SrTiO₃ peak (*) for three different azimuths in which the 424 (q_y), 206 ($+q_y$), and 602 ($-q_y$) DyScO₃ peaks are also seen. The period of the thickness fringes is inversely proportional to the film thickness. (b) Plot of the thickness fringe minimum position vs number for a section of the CTR. The film thickness is equal to $2\pi/\text{slope}$. The regularity of this period of the oscillations over a large region of reciprocal space and thickness oscillations extending far from the Bragg peak along the CTR show the high crystalline quality of the film.

(101) DyScO₃, the (001)_p SrTiO₃ plane is parallel to the (101) DyScO₃ plane, and the (100)_p SrTiO₃ plane aligns parallel to the (010) DyScO₃. The epitaxial relationship is (001)_p SrTiO₃||[101] DyScO₃ and [100]_p SrTiO₃||[010] DyScO₃, which is consistent with the epitaxial relationship found in DyScO₃ films grown on SrTiO₃.⁴⁷ Commensurate (001)_p SrTiO₃ films grown on (101) DyScO₃ substrates are thus strained by $(a_{\text{sub}} - a_{\text{film}})/a_{\text{film}} = 1.09\%$ along the [101] DyScO₃ and 1.19% along the [010] DyScO₃ (where a_{sub} is the in-plane spacing of the rectilinear surface net of the substrate and a_{film} is the lattice parameter of unstrained SrTiO₃).

The XRD data in Fig. 2(a) show the $20\ell_p$, $02\ell_p$, and $0\bar{2}\ell_p$ crystal truncation rods (CTRs) around the 204_p-type SrTiO₃ peaks from a 500 Å thick film. Finite thickness oscillations extend far in reciprocal space from the SrTiO₃ peak with a constant period [see Fig. 2(b)]. The regularity of the oscillations shown is typical for all of the films and indicates the presence of long range structural order and a smooth film surface, since the breadth of scattering of the CTR is inversely proportional to the roughness of the surface.⁴⁸ This quality of films is typically found in semiconductor-grade materials such as GaAs and related III-V semiconductors,^{49,50} but is less commonly observed for perovskite oxide materials.

In Fig. 2(a) it is apparent that there are three distinct positions for the DyScO₃ peak in these scans depending on

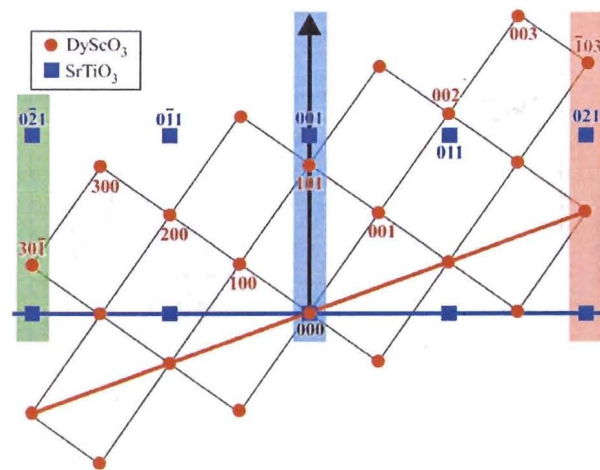


FIG. 3. (Color online) Schematic of the epitaxy of the SrTiO₃ (■) and DyScO₃ (●) lattice in reciprocal space. Along this axis the DyScO₃ lattice is canted at an angle of $\sim 3^\circ$ as compared to the SrTiO₃ lattice due to the different orientations of the $[\bar{1}01]$ DyScO₃ and $[001]_p$ SrTiO₃ directions. The tilt in the figure is exaggerated for clarity. The arrow shows the scan direction along the CTRs used for the scans in Fig. 2(a).

the in-plane direction. The three substrate peaks near the SrTiO₃ 204_p-type peaks are the DyScO₃ 424, 206, and 602 peaks. The epitaxial relationship between the SrTiO₃ lattice and the DyScO₃ lattice is represented in the schematic of reciprocal space shown in Fig. 3. The DyScO₃ reciprocal lattice is slightly tilted from the SrTiO₃ reciprocal lattice because the $[\bar{1}01]$ direction is not parallel to the normal of the $(\bar{1}01)$ plane in orthorhombic DyScO₃. As the y coordinate of the reciprocal lattice, q_y , is increased from the origin, the q_z position of DyScO₃ Bragg peak will be higher than that of the SrTiO₃ along the same CTR. The result can be seen in the top spectrum of Fig. 2(a), where the 206 DyScO₃ occurs at a larger q_z than the SrTiO₃ peak, and this azimuth is labeled as the $(+q_y)$ axis. If q_y is negative, then the q_z position of the 602 DyScO₃ peak is lower than the SrTiO₃ peak along the CTR. This is seen in the lower spectrum in Fig. 2(a) and this azimuth is labeled as the $(-q_y)$ axis.

B. Stoichiometry and crystalline quality

The SrTiO₃ films were investigated using RBS and channeling to measure the depth profile of the composition and the crystalline quality. The experiments were performed with 1.4 MeV He⁺ ions. The RBS and channeling results for a SrTiO₃ film on a (101) DyScO₃ substrate are shown in Fig. 4. Channeling was performed perpendicular to the surface of the substrate as well as inclined by an angle of 45° from the substrate normal along the [100], [001], and [121] directions of the substrate. Comparisons between the simulated and experimental data for a random scattering (nonchanneling) measurement showed that the Sr to Ti (Sr/Ti) ratio is 0.9–0.95 with a detection accuracy near 5%. The films are thus stoichiometric within the accuracy of the RBS measurement. The minimum yield of the SrTiO₃-film is estimated to be $\chi_{\text{min}} < 3\%$. This value is representative of a film with a high degree of structural perfection. The channeling measure-

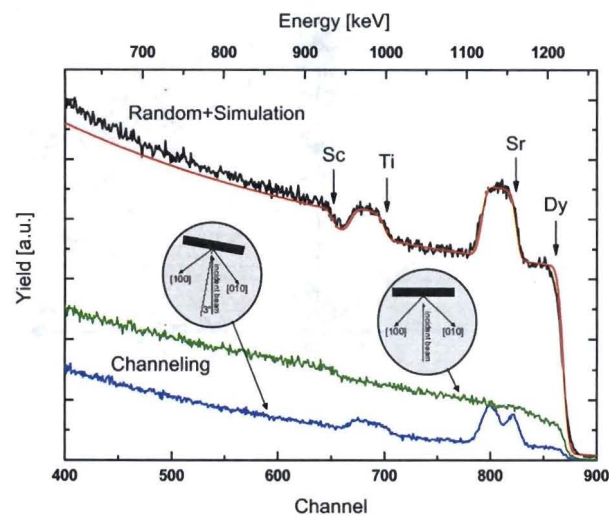


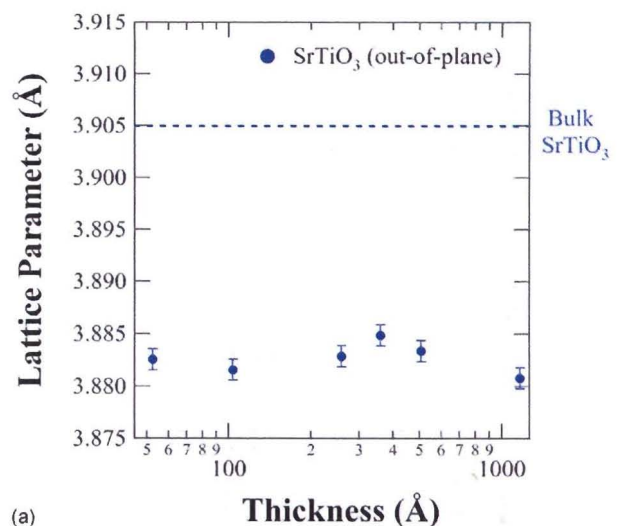
FIG. 4. (Color online) RBS measurement performed using He^+ ions with an energy of 1.4 MeV on a 500 Å thick SrTiO_3 thin film grown on (101) DyScO_3 . The plot shows three measurements: a random spectrum and two channeling spectra. The arrows on the random RBS spectra show the onset positions of the constituent elements. The simulation overlaid on the data is of a 410 Å thick strontium titanate film on DyScO_3 with a Sr:Ti ratio of 0.90. The two channeling spectra were made along different orientations. The one perpendicular to the plane of the substrate (0°), shows the maximum channeling for the SrTiO_3 film. The one inclined by an angle of $\sim 3^\circ$ from the surface normal, shows maximum channeling for the DyScO_3 substrate. These channeling measurements are indicative of the high structural quality of the heteroepitaxial SrTiO_3 film.

ments found that the (101) DyScO_3 substrates exhibit maximum channeling inclined from the substrate normal by an angle of $\sim 3^\circ$ which corresponds to the 2.8° tilt between the normal to the $(\bar{1}01)$ DyScO_3 plane and $[\bar{1}01]$ DyScO_3 direction.^{17,23,24,26,42,43} In contrast, the SrTiO_3 thin film shows a maximum channeling normal to the film and substrate surface. This corroborates the epitaxial relationship described previously.

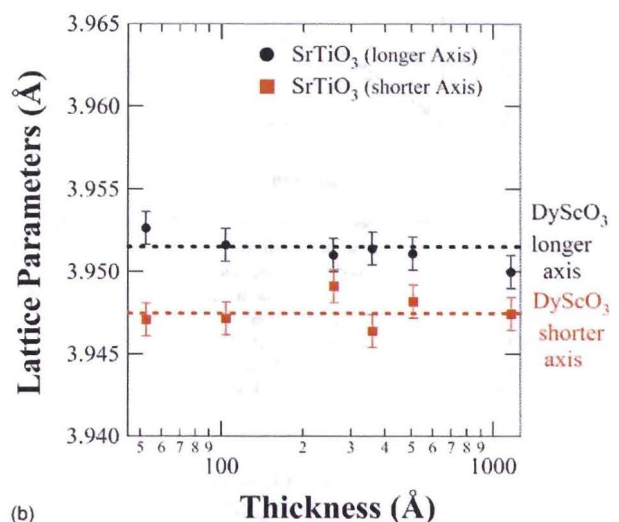
C. Critical thickness and strain relaxation

1. X-ray diffraction

The lattice parameters of SrTiO_3 were measured as a function of film thickness to identify the critical thickness for the onset of relaxation of the strained SrTiO_3 thin films. XRD data along the CTR were fit to determine the thickness of the films and the out-of-plane lattice constant of the SrTiO_3 .^{51,52} The in-plane lattice constants were then determined using the d spacings of several off axis peaks and the out-of-plane lattice constants. The lattice constants as a function of film thickness are shown in Fig. 5. The out-of-plane lattice constant does not change as a function of film thickness [Fig. 5(a)]. In Fig. 5(b), the in-plane lattice parameter of the SrTiO_3 is commensurate for the shorter in-plane axis (the $[\bar{1}01]$ DyScO_3 direction), but some relaxation is observed for films greater than 500 Å thick along the longer in-plane axis (the $[010]$ DyScO_3 direction). This indicates that the onset of relaxation (the critical thickness) for this system is between 350 and 500 Å. It is also important to note that even at



(a)



(b)

FIG. 5. (Color online) (a) The out-of-plane and (b) in-plane lattice constants of the SrTiO_3 films as a function of thickness. The lattice spacings of the DyScO_3 substrate and bulk SrTiO_3 are indicated by dashed lines. The out-of-plane lattice constants show very little change as a function of film thickness. A significant difference in the in-plane lattice constants is observed in accord with the rectangular underlying surface net of the (101) DyScO_3 substrate. The in-plane lattice spacings show no relaxation along the shorter axis of the substrate, but along the longer in-plane axis the films thicker than 350 Å begin to show some relaxation. The error bars indicate the accuracy of the lattice spacings, but the precision of the measurements is within the size of the solid symbols.

1000 Å, the film is still $\sim 90\%$ coherent along the longer axis and nearly 100% coherent along the shorter axis.

2. RHEED

The onset of relaxation deduced from the evolution of the RHEED patterns during film growth is consistent with the XRD results, though not as easy to discern. At the beginning of the film growth, Fig. 6(a), the RHEED pattern of the substrate shows spots on an arc. After 180 Å of SrTiO_3 has been grown [Fig. 6(b)] the RHEED pattern still shows small spots for the first-order diffraction rod. This pattern [Fig. 6(b)] also shows that the lattice constant of the SrTiO_3 is half

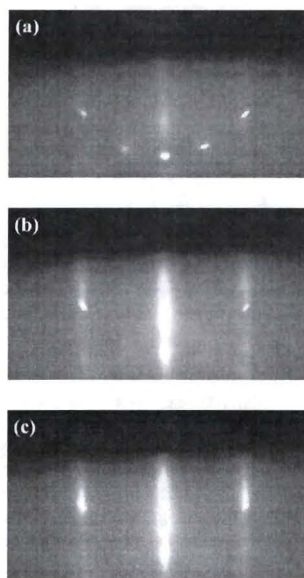


FIG. 6. RHEED patterns during the growth of the 500 Å thick SrTiO₃ film on DyScO₃ observed along the $[110]_p$ SrTiO₃ azimuth for (a) a bare DyScO₃ substrate just before growth, (b) after the growth of 180 Å of SrTiO₃, and (c) after the growth of 450 Å of SrTiO₃.

that of the DyScO₃, illustrated by the fact that the first-order diffraction spots in Fig. 6(b) are in the same position as the second-order diffraction spots of the bare (101) DyScO₃ substrate in Fig. 6(a). This also confirms the epitaxial relationship $[100]_p \text{SrTiO}_3 \parallel [010] \text{DyScO}_3$, as described previously. At a film thickness of 450 Å the first order diffraction rods have broadened [Fig. 6(c)], indicating that the film has started to relax. The exact onset of relaxation by RHEED is difficult to determine since the change is gradual, but by 450 Å the streaking of the first order diffraction rods is clear. This bounds the onset of relaxation to between 180 and 450 Å; thus the agreement between RHEED and XRD is good.

The equilibrium critical thickness was calculated by a mechanical balance equation corresponding to the equilibrium thickness at which it becomes favorable to introduce dislocations, as described by Matthews and Blakeslee.⁵³ To apply this equation it is necessary, however, to know the slip system that is active. The Burgers vector of a misfit dislocation was determined by both diffraction contrast imaging and high-resolution lattice imaging using transmission electron microscopy. The misfit dislocations are edge type and run along the $\langle 100 \rangle_p$ direction of SrTiO₃. The Burgers circuit in Fig. 7 shows that the Burgers vector is $a\langle 101 \rangle_p$, 45° inclined to the film-substrate interface. The projection of the Burgers vectors in the plane of the film-substrate interface is either $a[100]_p$ or $a[010]_p$. Some of the misfit dislocations are dissociated into two partials with the Burgers vectors of $a/2\langle 101 \rangle_p$, as shown in Fig. 7.

This information was used to calculate the equilibrium critical thickness. Poisson's ratio (ν) of SrTiO₃ was calculated to be $\nu \approx 0.23$ from $\nu = -s_{12}/s_{11}$ using the temperature dependent compliances of SrTiO₃ from Rupprecht and Winter⁵⁴ extrapolated to 650 °C. Using the Matthews–

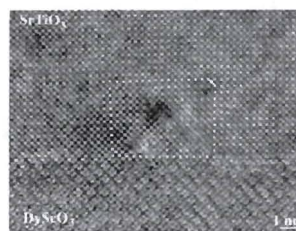


FIG. 7. Cross-sectional HRTEM micrograph taken along the $[010]_p$ SrTiO₃ zone axis of an 800 Å thick SrTiO₃ film showing a misfit dislocation core with a total Burgers vector of $a\langle 101 \rangle$, which is dissociated into two partials with Burgers vectors of $a/2\langle 101 \rangle_p$.

Blakeslee criterion with the $\langle 100 \rangle_p - \{011\}_p$ slip system and $\nu = 0.23$ gives a critical thickness of ~ 60 Å for a strain of $\epsilon = 1.14\%$, corresponding to the growth of SrTiO₃ on (101) DyScO₃. The discrepancy between the equilibrium (Matthews–Blakeslee) critical thickness at which it becomes energetically favorable to introduce dislocations and the experimentally observed critical thickness is not surprising because the experimentally observed critical thickness is kinetically limited by Peierls–Nabarro stress, dislocation nucleation, dislocation interactions, and other potential barriers impeding dislocation introduction, especially at the relatively low growth temperatures employed.^{55,56}

The film relaxation primarily along one direction [see Fig. 5(b)] was initially unexpected. Using the DyScO₃ lattice constants reported in the International Centre for Diffraction Data (ICCD) powder diffraction file, a cut along the (101) plane produces an in-plane rectilinear surface net with spacings of 3.9439 and 3.9444 Å at room temperature along the $1/2[\bar{1}01] \text{DyScO}_3$ and $1/2[010] \text{DyScO}_3$ directions, respectively.⁴² This creates a lattice mismatch of 0.996% along DyScO₃ $[\bar{1}01]$ and 1.009% along DyScO₃ $[010]$ with SrTiO₃ (3.905 Å), yielding a biaxial tensile strain with $\epsilon_{11} \approx \epsilon_{22}$ in unrelaxed films (where ϵ_{11} and ϵ_{22} are in-plane strains). The nominal difference of 0.0005 Å between the two orthogonal directions of the surface net is on the order of the accuracy of our x-ray diffractometer. The x-ray data on the DyScO₃ single crystal substrates used in this work, however, indicate in-plane surface net spacings of 3.9513 ± 0.0004 Å and 3.9475 ± 0.0003 Å along the $1/2[010]$ and $1/2[\bar{1}01]$ DyScO₃ directions, respectively. The difference of 0.0038 Å between the two is much larger than previously reported. This discrepancy may be attributed to differences in stoichiometry between our single crystals grown at the congruent melting composition,^{23,24} and the powder reported in the ICCD powder diffraction file.⁴² It is almost certainly the difference in spacings for the two orthogonal in-plane directions ($\epsilon_{11} \neq \epsilon_{22}$) that drives the anisotropy in the relaxation of the SrTiO₃ films. Relaxation can be seen in Fig. 5(b) to occur along the more strained in-plane direction first, as expected.

3. XRD rocking curves

The rocking curves, in ω , for these films show a full width at half maximum (FWHM) of the 002_p SrTiO₃ peak that ranges from 6.5 to 18 arc sec (0.0018°–0.0050°). As

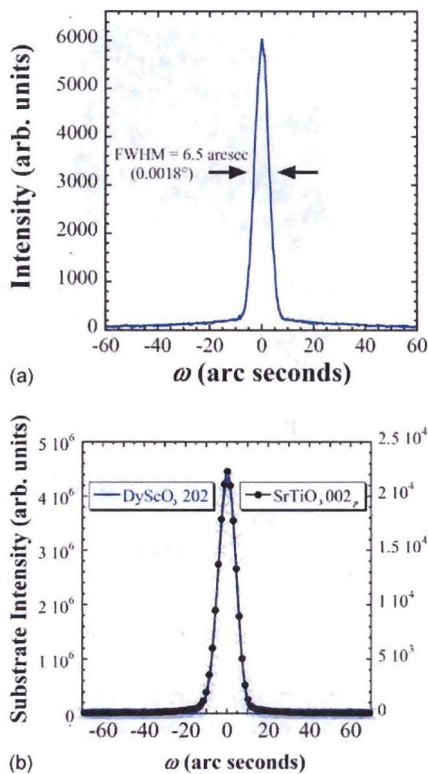


FIG. 8. (Color online) (a) Rocking curve of the SrTiO_3 002_p peaks for a 350 Å thick SrTiO_3 film. The FWHM is 6.5 arc sec (instrument limited). (b) Scaled rocking curves of the 002_p SrTiO_3 film peak and 202 DyScO_3 showing identical shapes.

Fig. 8(a) shows, the rocking curve FWHM of the 350 Å thick film is just 6.5 arc sec (0.0018°), which is the resolution limit of our high-resolution diffractometer. This is the narrowest rocking curve reported for any heteroepitaxial oxide thin film.⁵⁷ This structural quality is comparable to that of high quality silicon and germanium single crystals.^{58,59} Similar peak widths were found off axis and in the grazing-incident scattering measurements performed at the Advanced Photon Source, indicating that these films have a high degree of uniformity and structural perfection. This high crystalline quality is a consequence of the structural perfection of the DyScO_3 substrate, the template for epitaxial growth. If the rocking curve of the film and substrate are overlaid, as is done in Fig. 8(b), they have identical shapes and FWHM.

This rocking curve FWHM of our MBE grown SrTiO_3 film is the narrowest reported for SrTiO_3 in any form, including single crystals.^{60–63} Figure 9 overlays the rocking curve of the 002 peak of several commercial bulk SrTiO_3 single crystals grown by flame fusion (or the Verneuil process) and float zone techniques.²⁵ In preparing this figure we measured many commercial (001) SrTiO_3 single crystals²⁵ grown by flame fusion. The narrowest rocking curve of the SrTiO_3 crystals grown by flame fusion had a FWHM of 63 arc sec. In contrast the broadest, which was comparable to many of the substrates grown by this technique, had a FWHM of 391 arc sec. We also measured a (001) SrTiO_3 single crystal grown using the float zone technique. These typically have narrower rocking curves than those grown by flame fusion.⁶³

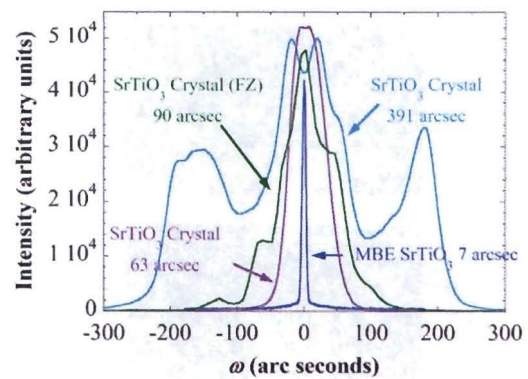


FIG. 9. (Color online) A comparison of the rocking curves for various bulk SrTiO_3 single crystals and our MBE grown SrTiO_3 thin film. Two of these rocking curves are from SrTiO_3 single crystals grown by the flame fusion method. These exhibit 63 and 391 arc sec FWHM rocking curves. The SrTiO_3 single crystal grown by the floating zone technique (labeled FZ) has a rocking curve FWHM of 90 arc sec. With a FWHM of 6.5 arc sec, the MBE grown SrTiO_3 film has a much narrower rocking curve than all of the bulk single crystals.

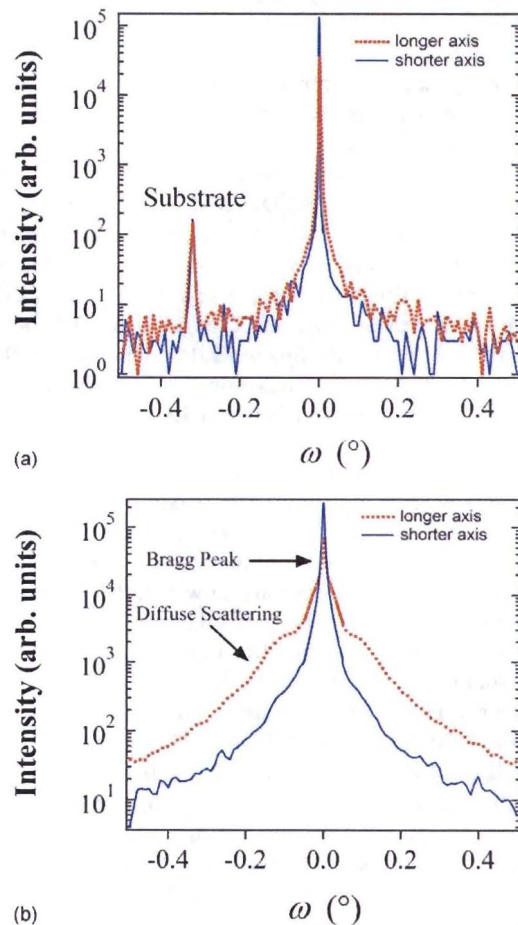


FIG. 10. (Color online) Rocking curves of the 002_p SrTiO_3 in orthogonal directions for (a) 350 Å and (b) 1000 Å thick films. The longer scan is taken along [010] DyScO_3 ; the shorter axis scan is taken along the [101] DyScO_3 . The peak labeled substrate in (a) arises from the shoulder of the 202 DyScO_3 peak.

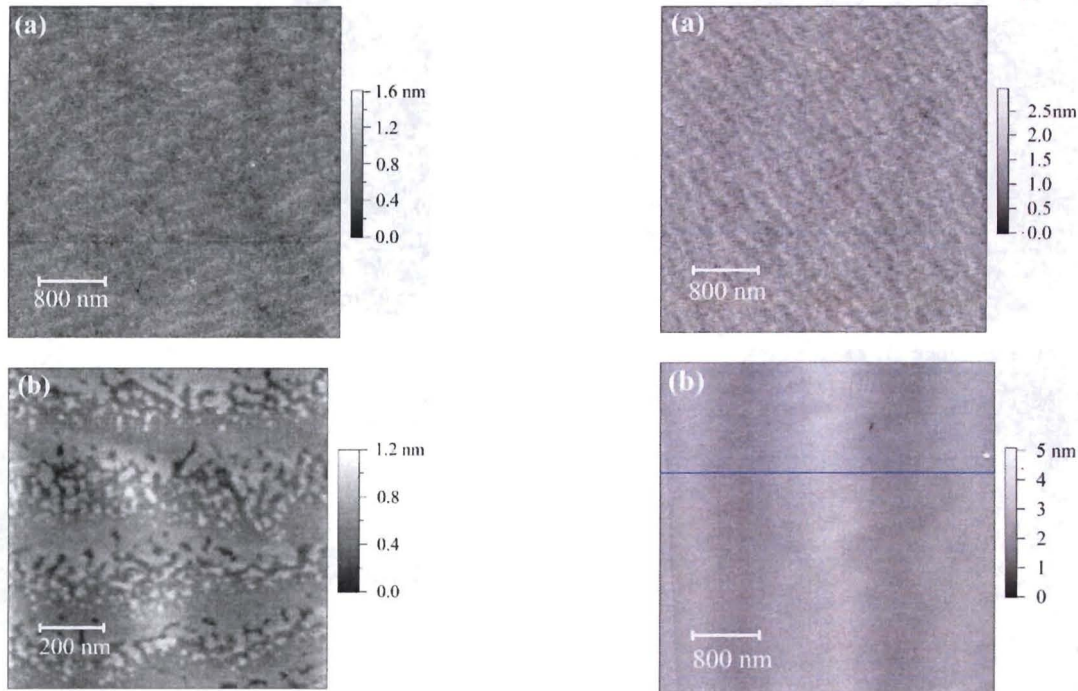


FIG. 11. AFM height images of (a) 250 Å and (b) 2000 Å thick films. Both films have ~ 4 Å unit cell high steps. The edges of the AFM images are aligned with $\langle 100 \rangle_p$ SrTiO₃ directions.

It had a rocking curve FWHM of 91 arc sec. The MBE grown SrTiO₃ films show a rocking curve FWHM approximately one order of magnitude smaller than these bulk SrTiO₃ single crystals, with FWHM as narrow as 6.5 arc sec. This narrow rocking curve is close to the fundamental limit, the intrinsic Darwin width of SrTiO₃.⁶⁴

The strain relaxation can also be observed via the shape of the rocking curves of these films (see Fig. 10). Films 350 Å and thinner have sharp, resolution-limited rocking curve widths. At thicknesses above the critical thickness, the rocking curves have components due to both Bragg and diffuse scattering. The sharp peak is attributed to the long range crystalline order of the unrelaxed portion of the film; the diffuse scattering is consistent with the existence of dislocations and local relaxation of the film as is typically seen in partially relaxed semiconductor films or for the heteroepitaxial growth of oxides on semiconductors.^{65–67} The onset of the diffuse scattering occurs for film thicknesses between 350 and 500 Å. The magnitude of the diffuse component is larger for the 1000 Å film. The rocking curves also reflect the anisotropy of the relaxation. In Fig. 10(a) the rocking curves along the two perpendicular in-plane axes are almost identical for the coherent films. In contrast, the 1000 Å thick film shows different shapes along the two orthogonal directions [Fig. 10(b)]. As expected, the rocking curve along the longer axis shows more diffuse scattering than the rocking curve along the shorter axis, while both curves have the same integrated areas. This is consistent with the relaxation occurring preferentially along the longer in-plane axis, were the film is under higher strain, in full agreement with the in-plane relaxation seen first along the more strained direction in Fig. 5(b).

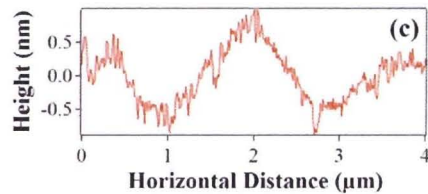


FIG. 12. (Color online) AFM height images of (a) a 350 Å thick SrTiO₃ film showing a very flat surface and (b) a 2000 Å thick film. (c) A horizontal line scan of the 2000 Å thick film reveals surface undulations. The line scan in (c) is along the longer DyScO₃ azimuth in which the SrTiO₃ film is more strained (the [010] in-plane direction of the DyScO₃ substrate).

4. Surface characterization

Evidence of the relaxation can also be seen in atomic force microscopy (AFM) images of the surface structure of the films. AFM images of all the films show terraces separated by 4 Å high steps. Two examples are shown in Fig. 11. The regular spacing of the steps indicates that films grow by either (1) the lateral propagation of their step edges (step flow) or (2) layer-by-layer growth (birth and spread).⁶⁸ The film surfaces have an rms roughness around 2.5 Å. Even the 2000 Å thick film, which was visibly cracked, showed well-defined steps and terraces between the cracks [Fig. 11(b)].

When imaged over a longer lateral scale, it was found that the coherent films are very smooth [Fig. 12(a)]. Once these films reach a sufficient thickness and begin to relax, the surfaces begin to form surface undulations [Figs. 12(b) and 12(c)]. This sinusoidal shape is commonly seen in strained semiconductor materials, and has been predicted and observed in films under both biaxial tensile and compressive stresses.^{69–77} This surface roughening mechanism also shows the anisotropy of the stress, in that these surface undulations are only in one direction, whereas three-dimensional mounds are typically observed for uniform in-plane strain.⁷³

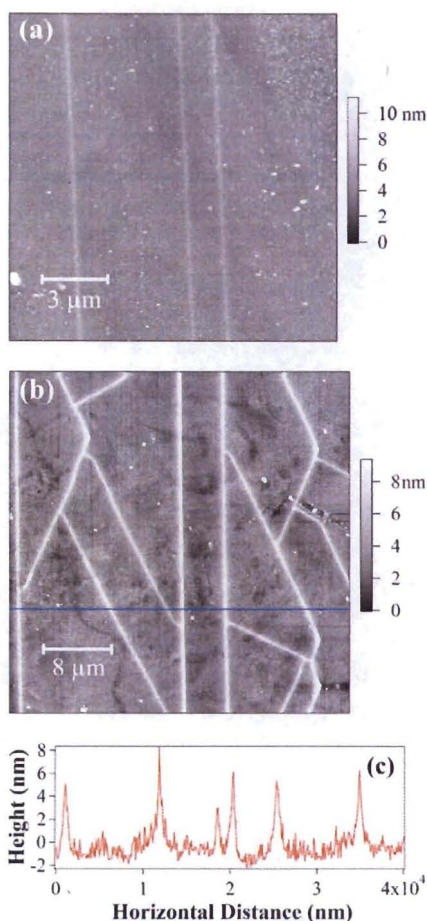


FIG. 13. (Color online) AFM height image of (a) 500 Å and (b) 1000 Å thick films showing surface cracks and dislocation traces. The line scan in (c) is along the longer DyScO₃ azimuth in which the SrTiO₃ film is more strained (the [010] in-plane direction of the DyScO₃ substrate).

The thicker films also show two additional features that are not seen in films below the critical thickness. There are protrusions above the surface of the film and also small steps resulting from dislocations (crosshatch) that appear as depressions in the surface; both can be seen in Fig. 13. On higher resolution examination the protrusions above the surface are found to be associated with cracks (Fig. 14). Near these cracks the SrTiO₃ juts above the surface of the films. Analogous cracks that appear raised in AFM images have been observed in SrFeO₃ films under biaxial tension.⁷⁸ A likely explanation is that the film has delaminated from the substrate near the crack to attain this height [Fig. 14(c)]. In the 500 Å thick film (just above the critical thickness), these surface features are all perpendicular to the longer axis (the axis with higher strain) and aligned parallel to $[\bar{1}01]$ DyScO₃ [Fig. 13(a)]. In the 1000 and 2000 Å thick films, the cracks are no longer limited to relieve the more strained in-plane direction and appear along different directions, though they are still mostly aligned perpendicular to the longer axis [Fig. 13(b)].

The surface steps resulting from the movement of the dislocations form a crosshatch pattern along the $[100]_p$ and $[010]_p$ SrTiO₃ directions [Fig. 13(b)]. Imaging of an inter-

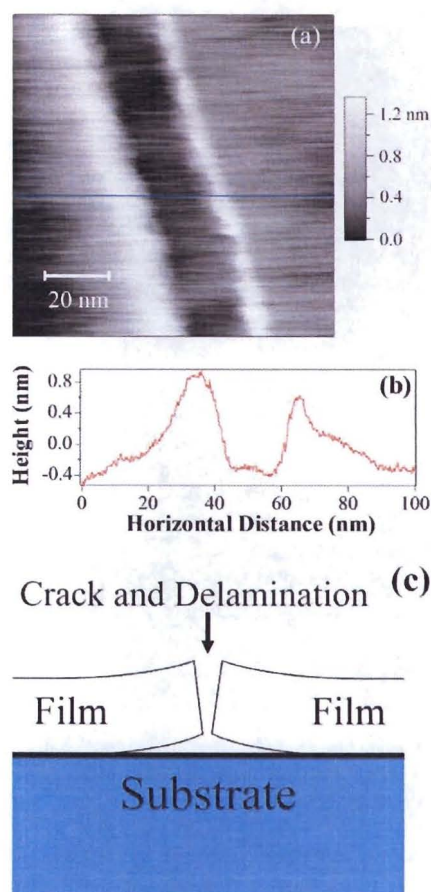


FIG. 14. (Color online) (a) Enlarged AFM image of cracks featured in Fig. 13 showing that the area near the crack is above the surface of the film. (b) Line scan along the longer in-plane direction (the [010] in-plane direction of the DyScO₃ substrate) showing the height of the crack region. (c) Schematic of the crack and delamination necessary to explain the height of the regions near the crack.

section between a crack and a surface step arising from dislocations shows that some of the crosshatch lines end at the cracks and do not appear on the other side of these cracks (Fig. 15). This means that the cracks form during growth of the film and not during the cooling of the sample, strongly suggesting that a primary mechanism through which the films relieve stress is through cracking, in addition to dislocation formation.

5. Annealing effects

To lower the dielectric loss of the as-grown SrTiO₃/DyScO₃ films, annealing was performed in 1 atm of flowing oxygen for 1 h prior to electrical measurements.¹⁸ To explore the effect of this reoxidation annealing on the film structure, *in situ* heating experiments in a controlled oxygen environment were performed. An as-deposited 100 Å thick SrTiO₃ film was heated to 750 °C and the 006_p SrTiO₃ peak was monitored *in situ* at the Advanced Photon Source while the oxygen partial pressure was changed from 10⁻⁸ to 10¹ Torr. Each time the pressure was changed, the film was allowed to equilibrate for 15 min. The position of the 006_p SrTiO₃ peak did not change during the experiment [Fig.

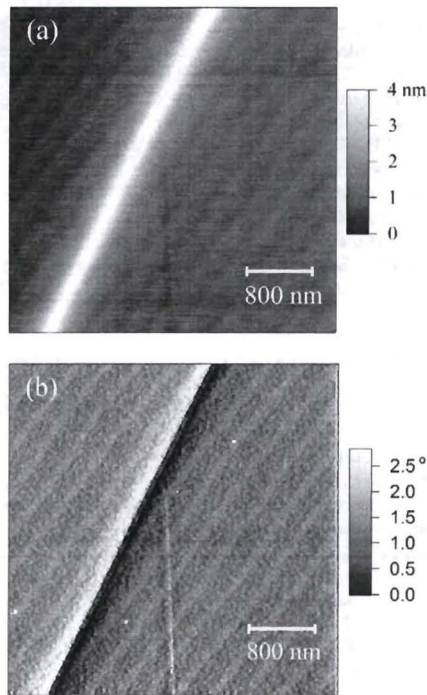


FIG. 15. Detailed AFM (a) height image and (b) phase image of the intersection between a crack and a straight step resulting from dislocations (crosshatch) in an 800 Å thick SrTiO₃ film illustrating that the crosshatch does not extend across the crack. Thus, the cracks must appear during the growth of the film. The scan (horizontal) direction is along the [010] in-plane direction of the DyScO₃ substrate, the longer in-plane direction.

16(a)]. This shows that the oxygen vacancy concentration did not affect the lattice parameter of these films. This is in sharp contrast to the commonly observed expanded lattice constant of SrTiO_{3-x} thin films grown by pulsed-laser deposition at low oxygen partial pressures,^{79,80} which expand further upon annealing in oxygen.⁸⁰ Similar insensitivity of the lattice constant of the SrTiO_{3-x} to oxygen vacancies, however, has been noted in experiments on bulk and single crystalline SrTiO_{3-x}.⁸¹⁻⁸³ For films below the critical thickness, no change in the strain state during the reoxidation annealing was observed. For further comparison, the rest of the samples were annealed at 700 °C for 1 h in flowing oxygen (1 atm) and the lattice parameters of these films were remeasured. For the thinner films the lattice constants do not change after annealing [Fig. 16(b)]. In contrast, the 500 and 1000 Å thick films relaxed further on annealing. This is not unexpected since the relaxation is kinetically limited; annealing would enable these films to relax and approach their thermodynamic equilibrium. It should be noted, however, that the amount of additional relaxation is modest even for the 1000 Å thick film, so that the film is still ~80% strained to the substrate lattice parameter.

IV. CONCLUSIONS

MBE grown epitaxial SrTiO₃ films on DyScO₃ have the highest reported crystalline quality of any heteroepitaxial oxide thin film (including perovskites) with rocking curves as narrow as 6.5 arc sec and extremely smooth surfaces, com-

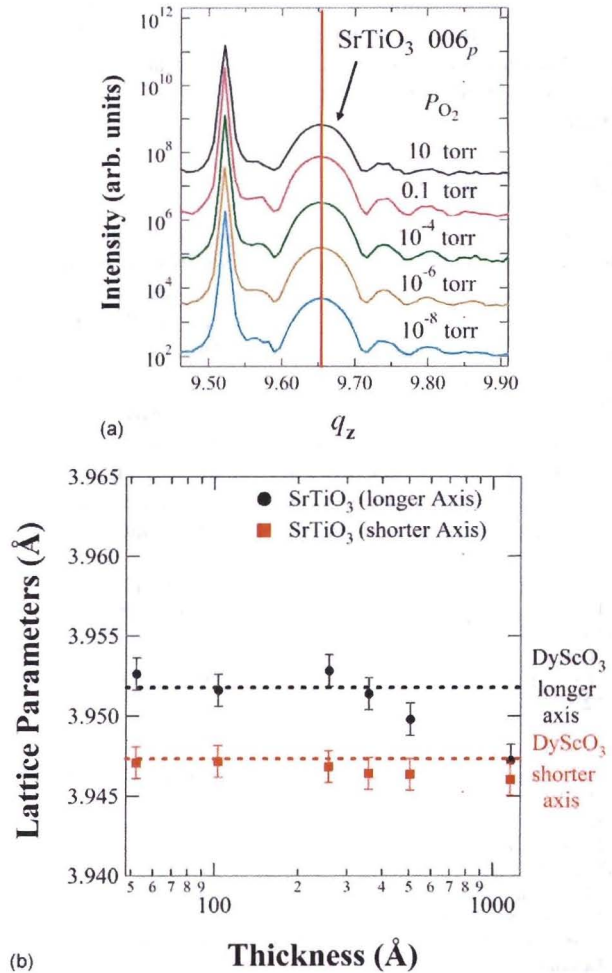


FIG. 16. (Color online) (a) Scans of the 006_p peak of a 100 Å thick SrTiO₃ film showing no discernible changes due to annealing the film at 750 °C in different oxygen partial pressures and (b) in-plane lattice parameters of the films after a reoxidation annealing in 1 atm of flowing oxygen for 1 h at 700 °C, showing a slight increase in the relaxation of the films thicker than the critical thickness.

parable to high quality semiconductor materials. This rocking curve width is an order of magnitude narrower than bulk SrTiO₃ single crystals. The critical thickness for the onset of strain relaxation in the SrTiO₃/(101) DyScO₃ system, for the MBE growth conditions used, was between 350 and 500 Å. Postannealing of the samples in different oxygen partial pressures caused no change in the lattice parameters for films below this critical thickness, indicating that oxygen vacancies are not affecting the lattice parameters of these SrTiO₃ films. Annealing did induce further relaxation in films above the critical thickness. The relaxation in this system was found to be anisotropic with almost all of the relaxation in an as-deposited 1000 Å film occurring along the more strained in-plane direction. This is associated with the in-plane anisotropy in the substrate. The relaxation in these films proceeds in a manner more similar to semiconductor materials such as GaAs and Si_{1-x}Ge_x, rather than typical perovskite materials (that contain much higher concentrations of structural defects). The introduction of dislocations in this system appears

to be difficult, resulting in the films cracking to relieve the strain energy from the epitaxial mismatch. This cracking of the film leads to raised surface features that are expected to be present in all epitaxial thin films that crack under tensile strain.

ACKNOWLEDGMENTS

The authors gratefully acknowledge helpful discussions with D.H.A. Blank, S.P. Baker, and V. Vaithyanathan, the use of the Center for Nanoscale Materials and Advanced Photon Source at Argonne National Laboratory, and the financial support of the National Science Foundation through Grant No. DMR-0507146, the Department of Energy through Grant No. DE-FG02-07ER46416, and the Office of Naval Research (ONR) through Grant No. N00014-03-1-0721 monitored by Dr. Colin Wood. Work at Argonne was supported by the U.S. Department of Energy, Office of Science, Basic Energy Sciences, under Contract No. DE-AC02-06CH11357.

- ¹G. A. Gehring and K. A. Gehring, *Rep. Prog. Phys.* **38**, 1 (1975).
- ²R. S. Beach, J. A. Borchers, A. Matheny, R. W. Erwin, M. B. Salamon, B. Everitt, K. Pettit, J. J. Rhyne, and C. P. Flynn, *Phys. Rev. Lett.* **70**, 3502 (1993).
- ³Q. Gan, R. A. Rao, C. B. Eom, J. L. Garrett, and M. Lee, *Appl. Phys. Lett.* **72**, 978 (1998).
- ⁴A. F. Devonshire, *Philos. Mag., Suppl.* **3**, 85 (1954).
- ⁵G. A. Samara, *Ferroelectrics* **2**, 277 (1971).
- ⁶G. A. Rossetti, Jr., L. E. Cross, and K. Kushida, *Appl. Phys. Lett.* **59**, 2524 (1991).
- ⁷K. Abe, N. Yanase, K. Sano, M. Izuha, N. Fukushima, and T. Kawakubo, *Integr. Ferroelectr.* **21**, 197 (1998).
- ⁸S. K. Streiffer, J. A. Eastman, D. D. Fong, C. Thompson, A. Munkholm, M. V. Ramana Murty, O. Auciello, G. R. Bai, and G. B. Stephenson, *Phys. Rev. Lett.* **89**, 067601 (2002).
- ⁹J. H. Haeni, P. Irvin, W. Chang, R. Uecker, P. Reiche, Y. L. Li, S. Choudhury, W. Tian, M. E. Hawley, B. Craigo, A. K. Tagantsev, X. Q. Pan, S. K. Streiffer, L. Q. Chen, S. W. Kirchoefer, J. Levy, and D. G. Schlom, *Nature (London)* **430**, 758 (2004).
- ¹⁰D. G. Schlom, L. Q. Chen, C. B. Eom, K. M. Rabe, S. K. Streiffer, and J.-M. Triscone, *Annu. Rev. Mater. Res.* **37**, 589 (2007).
- ¹¹K. J. Choi, M. D. Biegalski, Y. L. Li, A. Sharan, J. Schubert, R. Uecker, P. Reiche, Y. B. Chen, X. Q. Pan, V. Gopalan, L.-Q. Chen, D. G. Schlom, and C. B. Eom, *Science* **306**, 1005 (2004).
- ¹²J. M. Lock, *Proc. R. Soc. London, Ser. A* **208**, 391 (1951).
- ¹³H. Sato and M. Naito, *Physica C* **274**, 221 (1997).
- ¹⁴I. Bozovic, G. Logvenov, I. Belca, B. Narimbetov, and I. Sveklo, *Phys. Rev. Lett.* **89**, 107001 (2002).
- ¹⁵Throughout this manuscript we use the standard setting of space group No. 62, *Pnma*, to describe the crystallography of DyScO₃. Although some authors use this setting (Ref. 16), many others use the nonstandard setting *Pbnm* to describe the crystallography of DyScO₃ and other perovskites with the GdFeO₃ crystal structure (Ref. 17). The conversion from axes *a, b, c*, directions [*a b c*], or planes (*a b c*) in *Pnma* to *a', b', c'*, [*a' b' c'*], or (*a' b' c'*) in *Pbnm* is given by *a'=c*, *b'=a*, and *c'=b*.
- ¹⁶International Tables for Crystallography, in *Space Group Symmetry*, 5th ed., edited by T. Hahn (Kluwer, Dordrecht, 2002), Vol. A, p. 66.
- ¹⁷*Crystal structure data of inorganic compounds*, Landolt-Börnstein, New Series, Group III, Vol. 7, Pt. e, edited by K.-H. Hellwege and A. M. Hellwege (Springer-Verlag, Berlin, 1976), pp. 11–13.
- ¹⁸M. D. Biegalski, J. Haeni, S. K. Streiffer, V. Sherman, R. Uecker, P. Reiche, D. G. Schlom, and S. Trolier-McKinstry, *Appl. Phys. Lett.* **88**, 192907 (2006).
- ¹⁹DyScO₃ is orthorhombic. (101) DyScO₃ is a (100)_p pseudocubic surface.
- ²⁰R. Uecker, H. Wilke, D. G. Schlom, B. Velickov, P. Reiche, A. Polity, M. Bernhagen, and M. Rossberg, *J. Cryst. Growth* **295**, 84 (2006).
- ²¹P. Reiche, B. Heroneit, and D. Schulze, *Cryst. Res. Technol.* **20**, 845 (1985).
- ²²R. Uecker, P. Reiche, V. Alex, J. Doerschel, and R. Schalge, *J. Cryst. Growth* **137**, 278 (1994).
- ²³R. Uecker, M. Albrecht, B. Velickov, M. Bernhagen, and D. G. Schlom, *J. Cryst. Growth* **295**, 84 (2006).
- ²⁴B. Velickov, V. Kahlenberg, R. Bertram, and M. Bernhagen, *Z. Kristallogr.* **222**, 466 (2007).
- ²⁵CrysTec GmbH, Berlin, Germany.
- ²⁶M. D. Biegalski, J. H. Haeni, C. D. Brandle, A. J. Ven Grasis, S. Trolier-McKinstry, and D. G. Schlom, *J. Mater. Sci.* **20**, 952 (2005).
- ²⁷International Products Corporation, Burlington, NJ.
- ²⁸PM80 Headway Research Inc., Garland, TX.
- ²⁹Advanced Ceramics Corp., Strongsville, OH.
- ³⁰Aldrich-APL, Urbana, IL.
- ³¹Varian Associates, Vacuum Products Division, Lexington, MA.
- ³²C. D. Theis and D. G. Schlom, *J. Vac. Sci. Technol. A* **14**, 2677 (1996).
- ³³MKS Instruments, Wilmington, MA.
- ³⁴Swagelok Corp., Solon, OH.
- ³⁵Y. Horikoshi, M. Kawashima, and H. Yamaguchi, *Jpn. J. Appl. Phys.* **27**, 169 (1988).
- ³⁶J. H. Haeni, C. D. Theis, and D. G. Schlom, *J. Electroceram.* **4**, 385 (2000).
- ³⁷PANalytical B.V, Almelo, Netherlands.
- ³⁸G. B. Stephenson, D. D. Fong, M. V. Ramana Murty, S. K. Streiffer, J. A. Eastman, O. Auciello, P. H. Fuoss, A. Munkholm, M. E. M. Aanerud, and C. Thompson, *Physica B* **336**, 81 (2003).
- ³⁹J. A. Eastman, P. H. Fuoss, L. E. Rehn, P. M. Baldo, G.-W. Zhou, D. D. Fong, and L. J. Thompson, *Appl. Phys. Lett.* **87**, 051914 (2005).
- ⁴⁰JEOL Ltd., Tokyo, Japan.
- ⁴¹Veeco Metrology, LLC, Santa Barbara, CA.
- ⁴²Powder Diffraction File Card No. 27-220, International Centre for Diffraction Data, Swarthmore, 1986, p. 78.
- ⁴³J. M. Badie, *Rev. Int. Hautes Temp. Refract.* **15**, 183 (1978).
- ⁴⁴R. Wördenweber, E. Hollmann, R. Kutzner, and J. Schubert, *J. Appl. Phys.* **102**, 044119 (2007).
- ⁴⁵R. P. Liferovich and R. H. Mitchell, *J. Solid State Chem.* **177**, 2188 (2004).
- ⁴⁶R. J. Hill and I. Jackson, *Phys. Chem. Miner.* **17**, 89 (1990).
- ⁴⁷M. Boese, T. Heeg, J. Schubert, and M. Luysberg, *J. Mater. Sci.* **41**, 4434 (2006).
- ⁴⁸C. Thompson, C. M. Foster, J. A. Eastman, and G. B. Stephenson, *Appl. Phys. Lett.* **71**, 3516 (1997).
- ⁴⁹M. A. G. Halliwell, M. H. Lyons, and M. J. Hill, *J. Cryst. Growth* **68**, 523 (1984).
- ⁵⁰H. Queisser and E. E. Haller, *Science* **281**, 945 (1998).
- ⁵¹I. K. Robinson and D. J. Tweet, *Rep. Prog. Phys.* **55**, 599 (1992).
- ⁵²D. D. Fong and C. Thompson, *Annu. Rev. Mater. Res.* **36**, 431 (2006).
- ⁵³J. W. Matthews and A. E. Blakeslee, *J. Cryst. Growth* **27**, 118 (1974).
- ⁵⁴G. Rupprecht and W. H. Winter, *Phys. Rev.* **155**, 1019 (1967).
- ⁵⁵B. W. Dodson and J. Y. Tsao, *Appl. Phys. Lett.* **51**, 1325 (1987).
- ⁵⁶R. People and J. C. Bean, *Appl. Phys. Lett.* **47**, 322 (1985).
- ⁵⁷Y. Shibata, N. Kuze, M. Matsui, M. Kanai, and T. Kawai, in *Epitaxial Oxide Thin Films II*, edited by J. S. Speck, D. K. Fork, R. M. Wolf, and T. Shiosaki (Materials Research Society, Pittsburgh, 1995), Vol. 401, pp. 273–278.
- ⁵⁸R. Bubakova, J. Drahokoupil, and A. Fingerland, *Czech. J. Phys., Sect. A* **12**, 538 (1962).
- ⁵⁹R. Bubakova, J. Drahokoupil, and A. Fingerland, *Czech. J. Phys., Sect. A* **12**, 764 (1962).
- ⁶⁰H. J. Scheel, *Z. Kristallogr.* **143**, 417 (1976).
- ⁶¹H. J. Scheel, J. G. Bednorz, and P. Dill, *Ferroelectrics* **13**, 507 (1976).
- ⁶²S. B. Qadri, J. S. Horwitz, D. B. Chrisey, R. C. Y. Auyeung, and K. S. Grabowski, *Appl. Phys. Lett.* **66**, 1605 (1995).
- ⁶³P. I. Nabokin, D. Soutel, and A. M. Balbashov, *J. Cryst. Growth* **250**, 397 (2003).
- ⁶⁴C. G. Darwin, *Philos. Mag.* **43**, 800 (1922).
- ⁶⁵P. F. Miceli and C. J. Palmström, *Phys. Rev. B* **51**, 5506 (1995).
- ⁶⁶C. Kim, T. Spila, I. K. Robinson, and J. E. Greene, *J. Appl. Phys.* **83**, 7608 (1998).
- ⁶⁷A. R. Kortan, M. Hong, J. Kwo, J. P. Mannaerts, and N. Kopylov, *Phys. Rev. B* **60**, 10913 (1999).
- ⁶⁸D. Elwell and H. J. Scheel, *Growth of Crystals from High-Temperature Solutions* (Academic, New York, 1975).
- ⁶⁹R. J. Asaro and W. A. Tiller, *Metall. Trans.* **3**, 1789 (1972).
- ⁷⁰B. J. Spencer, P. W. Voorhees, and S. H. Davis, *Phys. Rev. Lett.* **67**, 3696 (1991).
- ⁷¹L. B. Freund and F. Jonsdottir, *J. Mech. Phys. Solids* **41**, 1245 (1993).

- ⁷²C. S. Ozkan, "Studies of morphological instabilities and defect formation in heteroepitaxial $\text{Si}_{(1-x)}\text{Ge}_x$ thin films via controlled annealing experiments," Ph.D. thesis Stanford University (1997).
- ⁷³C.-P. Liu, J. M. Gibson, T. I. Kamins, D. P. Basile, R. S. Williams, and D. G. Cahill, *Phys. Rev. Lett.* **84**, 1958 (2000).
- ⁷⁴A. Vaillonis, B. Cho, G. Glass, P. Desjardins, D. G. Cahill, and J. E. Greene, *Phys. Rev. Lett.* **85**, 3672 (2000).
- ⁷⁵C. W. Snyder, B. G. Orr, D. Kessler, and L. M. Sander, *Phys. Rev. Lett.* **66**, 3032 (1991).
- ⁷⁶B. G. Orr, D. Kessler, C. W. Snyder, and L. Sander, *Europhys. Lett.* **19**, 33 (1992).
- ⁷⁷H. Gao and W. D. Nix, *Annu. Rev. Mater. Sci.* **29**, 173 (1999).
- ⁷⁸H. Yamada, M. Kawasaki, and Y. Tokura, *Appl. Phys. Lett.* **80**, 622 (2002).
- ⁷⁹E. J. Tarsa, E. A. Hachfeld, F. T. Quinlan, J. S. Speck, and M. Eddy, *Appl. Phys. Lett.* **68**, 490 (1996).
- ⁸⁰T. Ohnishi, M. Lippmaa, T. Yamamoto, S. Meguro, and H. Koinuma, *Appl. Phys. Lett.* **87**, 241919 (2005).
- ⁸¹M. Kestigian, J. G. Dickinson, and R. Ward, *J. Am. Chem. Soc.* **79**, 5598 (1957).
- ⁸²W. Gong, H. Yun, Y. B. Ning, J. E. Greedan, W. R. Datars, and C. V. Stager, *J. Solid State Chem.* **90**, 320 (1991).
- ⁸³D. Tenne, I. E. Gonenli, A. Soukiassian, D. G. Schlom, S. M. Nakhmanson, K. M. Rabe, and X. X. Xi, *Phys. Rev. B* **76**, 024303 (2007).